SCIENCE CHINA
Chemistry

•REVIEWS•
SPECIAL TOPIC: Rechargeable Battery Technology

January 2024 Vol.67 No.1: 276–290
https://doi.org/10.1007/s11426-022-1506-1

# From atomistic modeling to materials design: computation-driven material development in lithium-ion batteries

Xiangrong Li[1], Xiang Chen[2], Qiang Bai[3], Yifei Mo[4] & Yizhou Zhu[1*]

[1]*Research Center for Industries of the Future and School of Engineering, Westlake University, Hangzhou 310030, China;*
[2]*Department of Chemical Engineering, Tsinghua University, Beijing 100084, China;*
[3]*College of Materials Science and Engineering, Taiyuan University of Technology, Taiyuan 030024, China;*
[4]*Department of Materials Science and Engineering, University of Maryland, College Park 20742, United States*

Received October 18, 2022; accepted January 10, 2023; published online January 13, 2023

As an advanced energy storage system, lithium-ion batteries play an essential role in modern technologies. Despite their ubiquitous success, there is a great demand for continuous improvements of the battery performance, including higher energy density, lower safety risk, longer cycling life, and lower cost. Such performance improvement requires the design and development of novel electrode and electrolyte materials that exhibit desirable properties and satisfy strict requirements. Atomistic modeling can provide a unique perspective to fundamentally understand and rationally design battery materials. In this paper, we review a few recent successful examples of computation-driven discovery and design in electrode and electrolyte materials. Particularly, we highlight how atomistic modeling can reveal the underlying mechanisms, predict the important properties, and guide the design and engineering of electrode and electrolyte materials. We have a conclusion with a discussion of the unique capability of atomistic modeling in battery material development and provide a perspective on future challenges and directions for computation-driven battery material developments.

**materials design, computation, modeling, batteries, electrolyte, electrode**

**Citation:** Li X, Chen X, Bai Q, Mo Y, Zhu Y. From atomistic modeling to materials design: computation-driven material development in lithium-ion batteries. *Sci China Chem*, 2024, 67: 276–290, https://doi.org/10.1007/s11426-022-1506-1

## 1 Introduction

In the pursuit of carbon neutrality and sustainable development of human society, the advancement of electrochemical energy storage systems is one of the key steps. Among various kinds of electrochemical energy storage systems, lithium-ion batteries exhibit high energy density, high power density, low self-discharge rate, and prolonged cycling life [1–3]. Therefore, lithium-ion batteries have been widely deployed from portable electronics to electric vehicles and grid-scale energy storage stations.

The remarkable success of lithium-ion batteries is intimately associated with material discoveries and developments. The discovery of layered material of $TiS_2$ as an intercalation cathode by Whittingham in 1972 enables the invention of the first rechargeable lithium-ion battery [2]. The milestone discovery of multiple oxide-based cathode materials by Goodenough, including layered $LiCoO_2$ [4], spinel $LiMn_2O_4$ [5], and olivine $LiFePO_4$ [4,6], laid the foundation for modern commercial lithium-ion batteries. In 1990, Dahn demonstrated that ethylene carbonate (EC) as an electrolyte solvent can form a stable protection film on a graphite anode spontaneously [7]. The stable cycling performance brought by EC leads to its ubiquitous role in liquid electrolytes for lithium-ion batteries. Recently, the discovery of superionic conductors of $Li_{10}GeP_2S_{12}$ [8] and $Li_7La_3Zr_2O_{12}$ [9] as promising solid-state electrolyte materials stimulates a series of research on all-solid-state batteries.

*Corresponding author (email: zhuyizhou@westlake.edu.cn)

Despite their tremendous success, rechargeable lithium-ion batteries still suffer from multiple shortcomings and remain issues to be solved. Mitigating the range anxiety for electric vehicles demands an increase in energy density and power density. Safety concerns about commercial liquid electrolytes drive the development of all-solid-state batteries, in which ceramic-based solid-state electrolytes can potentially provide intrinsic safety. The move to higher voltage electrodes requires the development and design of liquid electrolytes that can form a stable interphase and are compatible with electrodes [10].

The call for higher energy density, longer cycling life, and improved safety poses ever stricter requirements on electrode and electrolyte materials in lithium-ion batteries. Traditionally, material discoveries and developments are mostly driven either by the "trial-and-error" approach that is inefficient and expensive, or by the intuition from chemists that is difficult to generalize [11]. Therefore, the traditional material development paradigm cannot meet the demands and requirements of novel battery materials.

In the past few decades, computational approaches, especially atomistic modeling, have been demonstrated as emerging tools in the understanding and design of battery materials. By leveraging various computational tools, such as density functional theory (DFT) [12] and molecular dynamic (MD) simulations [13], atomistic modeling provides a unique microscopic perspective to fundamentally understand material properties and mechanisms [14–17]. Besides, high-throughput calculations can be performed on a large number of potential candidate materials in parallel, and then suggest the few most promising ones for experimental verification. Computation can also provide rational development strategies to predict, design, and screen novel battery materials. By doing *in silico* experiments, computation-driven approaches can reduce the time and labor cost of developing novel battery materials, accelerating the advancement of rechargeable lithium-ion batteries [11,16,18,19].

In this review, we highlight a few recent computation-driven research progress where atomistic modeling plays an indispensable role in designing novel battery materials, including cathodes, solid-state electrolytes, and solvents/salts/additives in liquid electrolytes. The understanding of ion-diffusion mechanism in rocksalt-type structures leads to the design of cation-disordered rocksalt transition-metal oxides as a new family of high energy density oxide cathode materials. In the recently developed halide-containing solid-state electrolytes family, first-principles calculations reveal how the unique anion sublattice and cation sublattice enable fast ionic diffusion, which inspires rational design strategies for novel halide-containing solid-state electrolytes. Phonon calculations demonstrate that the phonon-ion interactions are crucial to fast ion diffusion in solids, and phonon-related descriptors can be an efficient tool to explore potential fast ionic conductors. The continuous optimization of liquid electrolytes focuses on improving the electrochemical and chemical stability, while first-principles calculations help formulate rational design rules on selecting solvents, salts, and additives. These recent research advancements demonstrate that computation approaches play an essential role in providing fundamental understanding and rational design strategies for electrode and electrolyte materials in rechargeable batteries. In addition, we have witnessed a growing number of experimental validations of computation results [20–27]. These successful examples of joint experimental and computational studies indicate that computation-driven discovery has become an important paradigm in advancing battery materials.

## 2 Cation-disordered rocksalt materials: from microscopic diffusion channels to high energy density cathode materials

### 2.1 Diffusion pathways in rocksalt-type cathode materials

Layered lithium transition-metal oxide (LMO) materials, including $LiCoO_2$, Li(Ni, Mn, Co)$O_2$ (NMC), and Li(Ni, Co, Al)$O_2$ (NCA), have been the dominating type of cathode materials in rechargeable lithium-ion batteries for decades [28–34]. These layered LMO materials crystalize in the rocksalt-type structure, where lithium ions and transition-metal (TM) ions arrange in alternating layers along the (111) direction (Figure 1a–d). Upon cycling, the TM layers serve as the framework, while mobile lithium ions intercalate and deintercalate within lithium planes. To maintain structural integrity during cycling, TM ions are required to remain within their original planes even when the cathode is at a highly delithiated state. However, most cations fail to meet such requirements and would migrate into lithium layers upon charging. The thermodynamically driven migration of TM cations leads to the blocking effect on lithium-ion diffusion and thus the loss of reversible capacity, which is detrimental to the battery performance. Only a few exceptional TM cations, including Ni, Mn, and Co ions, have a strong tendency to remain in their original sites and to avoid cation mixing upon charging. The scarce choices of available TM cations greatly limit the design and development of novel cathode materials [25,28].

In 2014, Lee *et al.* [36] challenged the conventional idea that cation disorder in cathode materials is always detrimental to battery performance. On the contrary, by carefully choosing cations and designing the stoichiometry, they demonstrated that cation disorder rocksalt (DRX) materials can serve as promising electrode materials with high specific capacities and energy densities using the combination of experiment and *ab initio* computations. Based on the calculation results, Lee *et al.* [36] designed and successfully

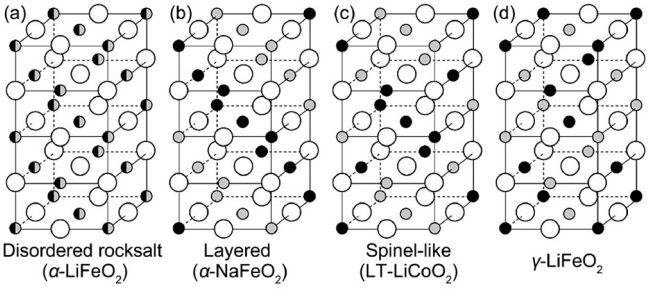


**Figure 1** The four common rocksalt-type LMO crystal structures. (a) The disorder rocksalt α-$LiFeO_2$ structure in which all cation sites are equivalent. (b) The layered structure (*α*-$NaFeO_2$ structure). (c) Spinel-like low-temperature (LT) $LiCoO_2$ structure. (d) The *γ*-$LiFeO_2$ structure. Large empty circles indicate oxygen sites, while small grey and black filled circles stand for lithium and transition-metal sites. (a–d) Reprinted with permission from Ref. [35], copyright 2014, Wiley-VCH.

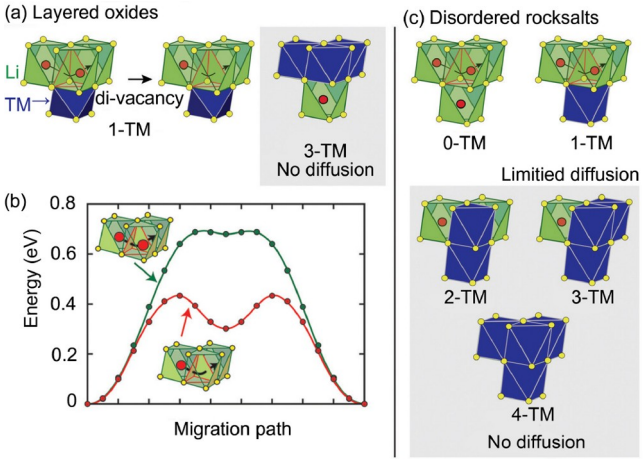


**Figure 2** In the rocksalt-type $Li_xMO_2$, $Li^+$ diffusion between neighbouring $O_h$ sites *via* an intermediate tetrahedral ($T_d$) site (*o*–*t*–*o* diffusion). (a) Layered $Li_xMO_2$ compounds exhibit 1-TM and 3-TM $T_d$ sites. Only 1-TM channels are responsible for $Li^+$ diffusion. (b) Li migration barriers between neighboring octahedral ($O_h$) sites in layered $Li_xMO_2$. Single vacancy diffusion has a much higher migration barrier than di-vacancy diffusion. (c) In disorder rocksalt materials, all types of tetrahedral clusters (0-TM, 1-TM, 2-TM, 3-TM and 4-TM channels) exist. In this case, 0-TM channels (and, to some extent, 1-TM channels) are responsible for $Li^+$ diffusion. (a, b) Reprinted with permission from Ref. [37], copyright 2013, American Chemical Society. (c) Reprinted with permission from Ref. [28], copyright 2019, The Royal Society of Chemistry (color online).

synthesized $Li_{1.211}Mo_{0.467}Cr_{0.3}O_2$ (LMCO) compound, which can transform from ordered structure to DRX in just a few charge-discharge cycling. The carbon-coated LMCO cathode material can deliver a remarkably high reversible capacity of ~660 Wh $kg^{-1}$, which is rarely achieved even in the layered Li–TM oxide. The discovery of DRX materials unlocks the possibility of using a much broader range of TM ions or their combinations as the redox centers, making them promising candidates for large-scale electric transportation and grid electrochemical energy storage applications.

The discovery and design of DRX materials are closely related to the understanding of lithium-ion diffusion mechanism in oxide cathode materials at the atomistic scale [28,36]. In rocksalt-type structures, lithium ions occupy octahedral sites and can diffuse to a neighboring vacant octahedral site through an intermediate tetrahedral site (Figure 2a). The energy of the transition tetrahedral site is critical to the migration barrier of the *o*-*t*-*o* path (Figure 2b) [28,36].

Based on the local environments, namely the number of TM ions in the four neighboring octahedral sites, the tetrahedral sites can be classified into different types from 0-TM to 4-TM [35,36]. In rocksalt-type oxide cathode materials, lithium usually diffuses *via* a di-vacancy fashion, which means at least one of the neighboring octahedral sites must be empty to activate lithium migration (Figure 2c). Therefore, only those tetrahedral sites with at most one TM-ion neighbor are available for lithium-ion diffusion. In other words, only 1-TM and 0-TM channels are effective diffusion channels [28,35].

Besides the occupancy of gate sites, another crucial factor governing the migration barrier is the size of the tetrahedral site (quantified by the tetrahedral height). In layered LMO materials, only 1-TM channels can accommodate lithium diffusion (Figure 2a). The ordered arrangement of cations results in relatively independent structural relaxation of the interlayer spacing. Therefore, the tetrahedral heights and migration barriers are almost independent of the TMs. The typical tetrahedral heights in layered LMOs are around 2.6–2.7 Å, which correspond to a migration barrier around 200 meV. However, when a fraction of TM ions migrates into the lithium layer during charging, the strong Columbic interaction between the migrated TM ions and oxygen ions results in the shrinkage of lithium layers. The migration barrier through a 1-TM channel increases to around 500 meV when the tetrahedral height drops to 2.35–2.40 Å (Figure 3) [36]. Consequently, a significant decrease in the lithium mobility and the loss of reversible capacity are observed.

In DRX materials, since TM ions and lithium ions are blended in a disordered fashion, the typical interlayer spacing is much smaller than that between the lithium layers in layered LMOs. Therefore, 1-TM channels in DRX materials are generally considered to be inaccessible due to the high migration barrier. However, the disordered cation sublattice implies a statistical distribution of tetrahedral sites with various local environments. The 0-TM channels, which are absent in layered LMO materials, become the major diffusion channels in DRX materials. First-principles calculations show that the di-vacancy diffusion barrier along 0-TM channel remains as low as 300 meV even when the tetrahedral height is below 2.4 Å (Figure 3) [28,36].

## 2.2 Guiding principles in designing DRX materials

Thermodynamic stability and ionic diffusivity are two important factors that need to be considered in the design of

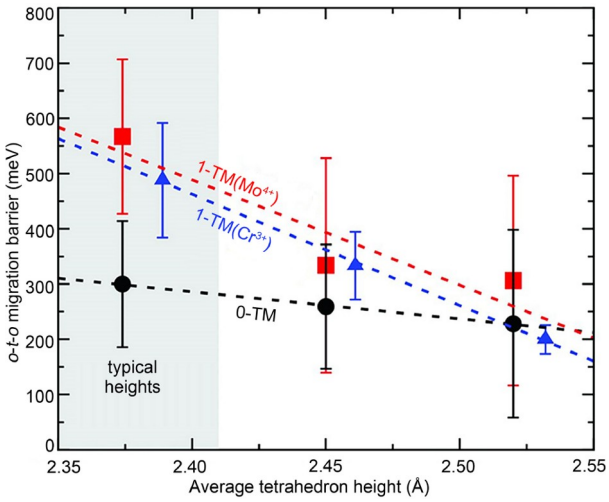


**Figure 3** Calculated Li migration barriers along 1-TM channels (red squares: one $Mo^{4+}$ neighbor; blue triangles: one $Cr^{3+}$ neighbor), and along 0-TM channels (black circles) as a function of the average tetrahedron height in model disordered $Li_2MoO_3$ and disordered $LiCrO_2$ structures. Error bars represent standard deviations, and the shaded area highlights the typical range of tetrahedron heights in disordered materials. Reprinted with permission from Ref. [36], copyright 2014, American Association for the Advancement of Science (color online).

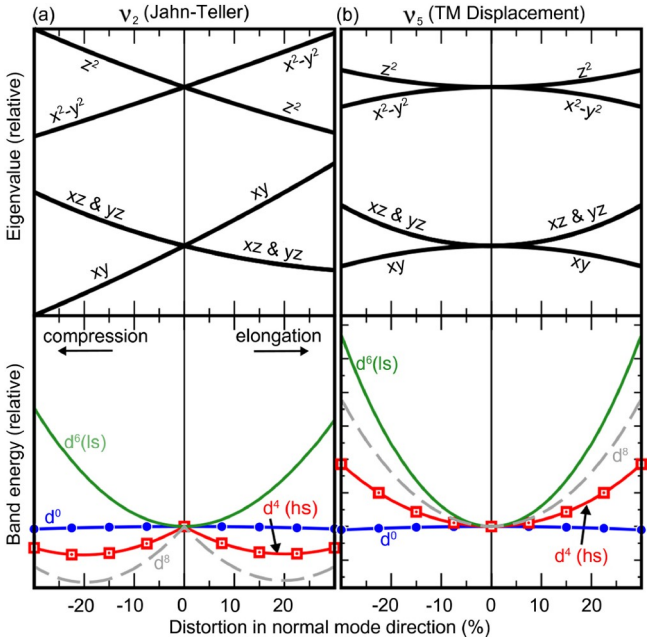


**Figure 4** Change of the electronic states (top) and the band energy (bottom) upon distortion of an octahedral TM site in the direction of (a) the Jahn–Teller mode ($v_2$) and (b) the TM-displacement mode ($v_5$). The band energies for four electronic configurations are shown: $d^0$ (blue circles), $d^4$ high spin (hs, red squares), $d^6$ low spin (ls, green line), and $d^8$ (gray dashed line). The labels in the top panels indicate the TM *d* orbitals that contribute most to distortions along the *z* direction. (a, b) Reprinted with permission from Ref. [39], copyright 2017, American Physics Society (color online).

DRX materials [25,28,38]. The tolerance to cation disorder determines the thermodynamic stability and synthesizability, while the ionic diffusivity is governed by the percolation and long-range diffusion of lithium ions [28].

In different DRX materials, the tolerance to cation disorder is strongly affected by the choice of TM cations. Cation disordering is observed even when a large mismatch in ionic radii and valence states is present (such as $LiNi_{0.5}Ti_{0.5}O_2$) in DRX materials [28]. Such a large cation mismatch in charge and size leads to strong local distortions from the ideal octahedral configuration. Urban *et al*. [39] revealed that the electronic structures of TM cations, especially the *d*-electron configurations, are closely related to the tolerance to cation disorder and local structural distortion. First-principles calculations reveal that the degenerate $t_{2g}$ and $e_g$ states will split under Jahn–Teller distortion or the TM-displacement distortion. The trend of band energy change depends on the *d* electron configurations [39]. The Jahn–Teller distortion either increases or decreases the band energy (Figure 4a), while the TM displacement distortion always leads to band energy increase (Figure 4b). TM ions with low-spin $d^6$ configurations (such as $Co^{3+}$, $Ni^{4+}$) possess filled $t_{2g}$ shells, and exhibit the highest energy penalty under local distortions (Figure 4b). By contrast, TM ions with $d_0$ configurations (such as $Ti^{4+}$ and $Zr^{4+}$) have no *d* electrons and their band energy is determined by the lower-lying oxygen-dominated orbitals (Figure 4b). Therefore, $d_0$ ions are quite tolerant to local site distortions, and can best accommodate the cation disorder even when the cation size mismatch is large. The necessity of including $d_0$ cations in forming DRX materials is verified by multiple synthesis experiments. Successful examples include $Li_{1.211}Mo_{0.467}Cr_{0.3}O_2$, $Li_{1.2}Mn_{0.4}Ti_{0.4}O_2$ and $Li_{1.2}Mn_{0.4}Zr_{0.4}O_2$, where $Mo^{6+}$, $Ti^{4+}$ and $Zr^{4+}$ act as the $d_0$ cation stabilizers, respectively [36,39].

Another important factor in designing DRX materials is that the material must enable macroscopic lithium diffusion [28,40]. The low migration barrier through 0-TM channels allows facile single-ion hopping but is no guarantee of fast long-range macroscopic diffusion [36]. In DRX materials, there is a statistical distribution of tetrahedral sites with different local environments. Only if the 0-TM channels form an interconnecting and percolating network, will the material exhibit measurable macroscopic current [28].

To study the governing factors of lithium percolation, Urban *et al*. [35] performed Monte Carlo simulations to reveal the influence of cation disorder and Li/TM ratio on lithium percolation. Under the ideal solution limit, the critical lithium content ($x_c$) for lithium percolation through 0-TM channels is around 1.1 per formula (Figure 5a), which corresponds to 10% lithium excess. When the cation configurations deviate from ideal solutions, and form layered, spinel-like, or $\gamma$-$LiFeO_2$-type sublattice ordering, the $x_c$ for the percolation changes to 1.09 (Figure 5b), 0.77 (Figure 5c), and 1.33 (Figure 5d), respectively. The critical lithium content for one Li per formula unit (1 Li per formula) to be accessible follows a similar trend.

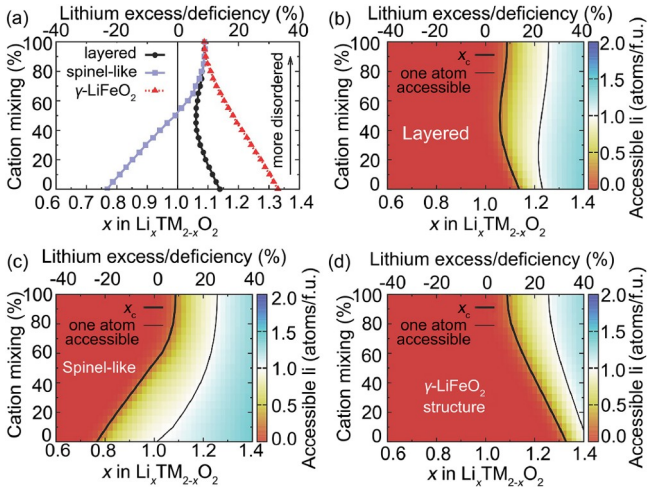


**Figure 5** (a) Critical lithium concentrations ($x_c$) for 0-TM Li percolation. (b–d) For one Li per formula unit (1 Li per formula) to be accessible *via* 0-TM channels as a function of the overall lithium content and the degree of cation mixing in $Li_xM_{2-x}O_2$ compounds with the layered ($\alpha$-$NaFeO_2$), spinel-like (LT-$LiCoO_2$) and $\gamma$-$LiFeO_2$ structure, respectively. Structure-specific $x_c$ values are indicated by thick black contour lines. Compositions failing to the left of these contour lines are not 0-TM percolating. Thin lines indicate the compositions at which one Li per formula unit becomes 0-TM accessible. (a–d) Reprinted with permission from Ref [35], copyright 2014, Wiley-VCH (color online).

As revealed in Monte Carlo simulations, lithium excess is essential for lithium percolation even under the ideal solution limits. High lithium content is beneficial for the lithium percolation and power density, but it would negatively impact the TM content and redox capacity. Therefore, the choice of desirable lithium content needs to balance the lithium diffusivity and capacity. The typical lithium concentration in DRX materials is usually between 1.1 to 1.3 lithium per formula [35].

The degree of cation disorder strongly influences the lithium diffusivity in DRX materials. Cation sublattice in spinel-like structure contains the most abundant 0-TM channels, and therefore favors the lithium percolation. By contrast, cation sublattice in $\gamma$-$LiFeO_2$-type structures has the lowest fraction of 0-TM channels, which hinders the formation of percolating networks for lithium diffusion [35]. Ji *et al*. [38] demonstrated the importance of short-range ordering in cation sublattice by comparing the performance of two DRX materials $Li_{1.2}Mn_{0.4}Zr_{0.4}O_2$ and $Li_{1.2}Mn_{0.4}Ti_{0.4}O_2$. Despite the identical Mn content, Li content, and $d^0$ ($Zr^{4+}$/$Ti^{4+}$) metal content, the reversible capacity of $Li_{1.2}Mn_{0.4}Ti_{0.4}O_2$ (0.79 per formula) is much higher than that of $Li_{1.2}Mn_{0.4}Zr_{0.4}O_2$ (0.52 per formula). Both calculations and experimental characterizations confirmed that the major difference between the two materials is the short-range order. Compared with $Li_{1.2}Mn_{0.4}Ti_{0.4}O_2$, $Li_{1.2}Mn_{0.4}Zr_{0.4}O_2$ deviate more from the random limit with undesirable short-range ordering. A decrease of 0-TM channels leads to a less percolated diffusion network and thus lower reversible capacity [38].

Following the aforementioned design principles, Lun *et al*. [25] synthesized three prototype compositions with increasing number of TM species to evaluate their high-entropy DRX design strategy. Although the same long-range order is retained in all compounds, the undesirable short-range order systematically decreases as the number of TM increase. Consequently, the energy density and rate capability also increase as the entropy increases. A compatibility analysis on multiple cations was performed to guide the choice of redox cations. And such design principles were validated by the successful synthesis of phase-pure DRX compound with up to twelve TM species.

## 3 Ionic diffusion and phonon properties: understand and design fast ionic conductors from lattice dynamics perspective

All-solid-state batteries are a promising next-generation energy storage system. The ceramics-based solid-state electrolyte materials are nonflammable and can potentially address the safety issues of current lithium-ion batteries [26,41,42]. Besides, the wide electrochemical stability windows can potentially enable high-voltage electrodes and thus achieve higher energy density. A key challenge in realizing ASSBs is to develop solid-state electrolyte materials [43]. An ideal solid-state electrolyte should have high ionic conductivity, low electronic conductivity, a wide electrochemical window and good compatibility with electrode materials [26,41,44].

Achieving high ionic conductivity in solid-state inorganic materials is challenging. Most solid-state inorganic materials only exhibit lattice vibration (phonon) at room temperature, and few atoms show the long-range diffusion [45]. By contrast, superionic conductors are a type of rare solid-state materials where certain ions can achieve a long-range diffusion under room temperature, and their ionic conductivity is comparable to ionic conductivity in liquids [46]. Despite decades of research, there are still only a handful of known solid-state electrolyte materials. Therefore, understanding and designing solid-state electrolyte materials are essential for the development of all-solid-state batteries [15,25,44,47,48].

Similar to DRX materials, the high ionic conductivities in solid-state electrolytes are closely related to the ion diffusion mechanisms at the atomistic scale, which is governed by the energy landscape when mobile lithium ions diffuse within the crystalline lattice [49–51]. The energy landscape strongly depends on the interactions between lithium ions and the surrounding frameworks, especially the anion sublattice. Such interactions can be ascribed to the phonon-ion interactions from the lattice dynamic perspective [45,51–53].

The softer and more polarizable anion sublattice benefits

the ion conduction by reducing the migration enthalpy ($\Delta H_m$) [52–55], as the weaker bonding between mobile lithium ions and anions broadens the oscillation of diffusion ions, therefore yielding a flat energy landscape with low activation energy for ion hoping (Figure 6a). Substituting polarizable anions to soften the crystal lattice have been frequently used to improve ionic conductivities [56], as exemplified in LISICONS of $Li_{3.2}Ge_{0.2}P_{0.8}X$ (X=O, S) [57,58], NASICON of $LiTi_2(PX_4)_3$ (X=O, S) [59,60], argyrodites of $Li_6PA_5X$ (A=S, O; X=Cl, I) [52,61,62] and lithium halides of $Li_3ErX_6$ (X=Cl, I) (Figure 6b) [63]. While the softer lattice is associated with the reduced $\Delta H_m$, the simultaneously decreased pre-factor due to the decline of the attempt frequency and migration entropy can limit or even reverse the enhancement of conductivities [52,53,58,63,64], which corresponds to the Meyer–Neldel rule [65,66]. Such compensation between the activation energy and pre-exponential factor has been observed in many lithium-ion conductors (Figure 6c–e) [56,58], and may result in the maximum conductivity at the intermediate composition upon continuously softening the lattice [52]. Thus, optimizing the conductivity through the lattice dynamics aspect should balance the compensation between the activation energy and the pre-factor. LGVPO refers to a series of compounds, including both the LGPO ($Li_{3.2}Ge_{0.2}P_{0.8}O_4$, $Li_{3.4}Ge_{0.4}P_{0.6}O_{0.4}$, $Li_{3.6}Ge_{0.6}P_{0.4}O_4$ and $Li_{3.8}Ge_{0.8}P_{0.2}O_4$) and LGVO ($Li_{3.2}Ge_{0.2}V_{0.8}O_4$, $Li_{3.4}Ge_{0.4}V_{0.6}O_4$, $Li_{3.6}Ge_{0.6}V_{0.4}O_4$ and $Li_{3.8}Ge_{0.8}V_{0.2}O_4$) system (Figure 6c).

Since the phonon–$Li^+$ interactions can impact the ionic transport, lattice dynamics can be utilized as a predictor to search and optimize new lithium-based fast ionic conductors. The phonon band center has been proposed to describe the dynamics of mobile $Li^+$ [54,55,58,64,67], which refers to a phonon frequency weighted by the phonon density of states (PDOS). Since the PDOS can be rapidly calculated through *ab initio* or classical simulations [64,68], high-throughput computations can be employed to search the fast ionic conductors with the phonon band center as a descriptor. Shao-Horn *et al*. [54] investigated the effect of the lithium band center on the ionic transport in the family of LISICON and olivine materials. Fast ionic conductors with low migration energies are found to be associated with the small phonon band center (Figure 7a, b). Based on the descriptor, multiple compounds (*e.g.*, $Li_{3.25}Ge_{0.25}P_{0.75}S_4$, $LiMgAsO_4$, and $LiInGeO_4$) were selected as promising ionic conductors from the LISICON and olivine family. Muy *et al*. [55] further extended the candidate pool from certain material family to ~14,000 lithium-containing structures of the Materials Project database. By computationally screening the candidates using the lithium band center (<35 meV) and other criteria, several new fast ionic conductors were suggested as good candidate materials for lithium-ion batteries (Figure 7c). One of the proposed compounds, $Li_3ErCl_6$, was synthesized and characterized experimentally with high ionic conductivity

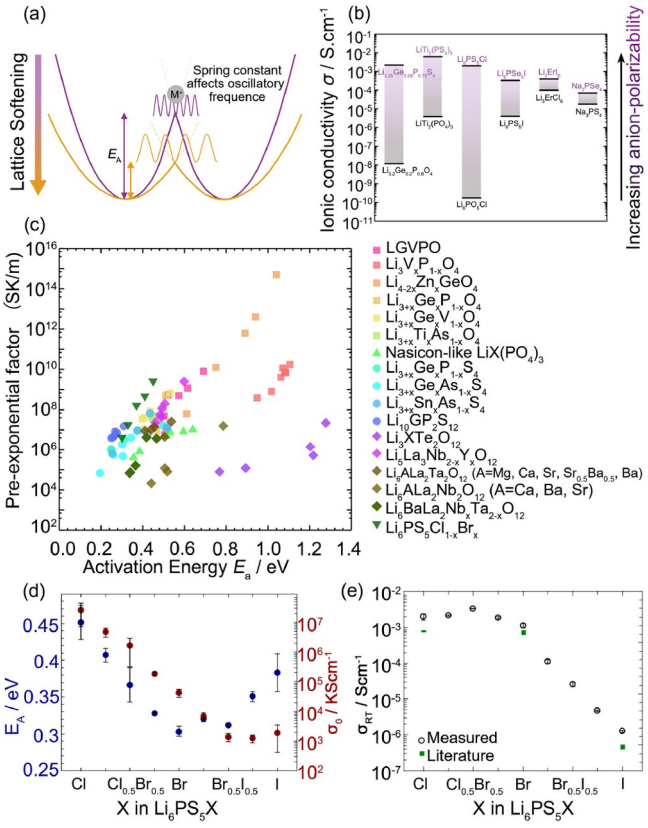


**Figure 6** (a) Schematic of the effect of lattice softness on the energy landscape of mobile ions $M^+$ upon jumping. (b) Lithium-ion conductivities of materials (*e.g.*, LISICONS of $Li_{3.2}Ge_{0.2}P_{0.8}X$ (X=O, S), NASICON of $LiTi_2(PX_4)_3$ (X=O, S), argyrodites of $Li_6PA_5X$ (A=S, O; X = Cl, I) and lithium halides of $Li_3ErX_6$ (X=Cl, I)) with increasing the anion polarizability by the substitution. (c) Relationship between the pre-factor and the activation energies of different material classes. (d) Experimentally measured activation energies and the pre-factor of the argyrodite $Li_6PS_5X$ (X=Cl, Br, I) with increasing the lattice softness by anion substitution. (e) Lithium conductivity of the argyrodite $Li_6PS_5X$ (X=Cl, Br, I) with increasing the lattice softness by anion substitution. (a, d, e) Reprinted with permission from Ref. [52], copyright 2017, American Chemical Society. (b) Reprinted with permission from Ref. [56], copyright 2021, Wiley-VCH GmbH. (c) Reprinted with permission from Ref. [58], copyright 2018, American Chemical Society (color online).

(0.33 mS $cm^{-1}$ at 300 K), validating their computational scheme (Figure 7d). As a result, the computational studies based on the phonon-related descriptors are demonstrated as an efficient tool to explore the fast ionic conductors through the lattice dynamics perspective [55].

In conclusion, the fast ionic diffusion of lithium ions within solid-state electrolyte materials is dictated by the interactions with the framework. Recent computation studies discovered that the lattice vibration property, namely the phonon properties, is strongly correlated with ionic diffusion properties. Thus, phonon-related descriptors can be promising computational tools to screen, validate and design novel fast ionic conductors.

Despite the achieved progress, the conceptional theory that correlates the phonon interactions to ionic conductivity is to

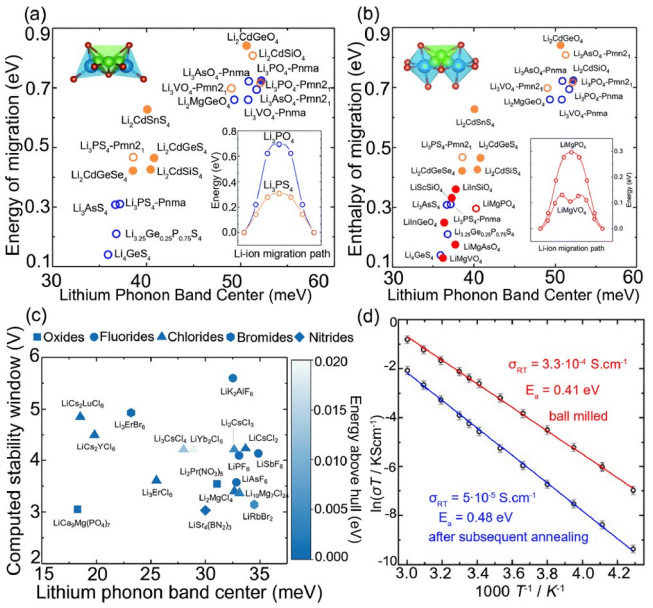


**Figure 7** High-throughput search for fast ionic conductors with low activation energies from (a) LISICON-related materials. (b) Lithium olivine. (c) Materials Project database, utilizing lithium phonon band center as a descriptor. (d) Experimentally characterized Arrhenius plot of the predicted $Li_3ErCl_6$. (a, b) Reprinted with permission from Ref. [54], copyright 2018, The Royal Society of Chemistry. (c, d) Reprinted with permission from Ref. [55], copyright 2019, The Authors (color online).

be developed [49,51,56]. There are still open questions relating the phonons to ionic transport. For example, is it possible to identify the certain phonon mode to promote the diffusion instead of utilizing the average vibration frequency, or can we even break the Meyer–Neldel rule to boost the conductivity? A better understanding of the phonon properties of the diffusion will benefit the computational material design of fast ionic conductors through the lattice dynamics perspective.

## 4 Halide-based solid-state electrolytes: the interplay between cation and anion sublattice

Halide-based solid-state electrolytes are a group of emerging materials that have received growing research interest in the past few years. Previously, most research efforts on solid-state lithium-ion conductors were devoted to oxides and sulfides. Sulfide-based solid-state electrolytes show high ionic conductivity, but they suffer from narrow electrochemical stability windows and poor moisture stability [48]. Oxide-based solid-state electrolytes exhibit better electrochemical compatibility with electrodes, but they have relatively low ionic conductivity at room temperature and undesirable mechanical properties [1].

The newly developed halide-based solid-state electrolytes, such as $Li_3YCl_6$ [69], $Li_3YBr_6$ [69], $Li_3InCl_6$ [70], and $Li_2ZrCl_6$ [71], have multiple advantages. They can achieve a high ionic conductivity under room temperature. For example, a recent study reported that the room-temperature ionic conductivity of 7.2 mS $cm^{-1}$ was achieved in $Li_3Y(Br_3Cl_3)$ [72]. Besides, halide-based materials generally have wide electrochemical windows, especially the good compatibility with most high-voltage cathode materials [73]. These ideal properties make halide-based solid-state electrolytes promising candidates for all-solid-state batteries.

Uncovering the ionic diffusion mechanism is crucial for understanding and design of novel halide-based solid-state electrolytes. Most solid-state electrolytes are ionic materials, and their crystal structures can be partitioned into cation sublattice and anion sublattice. In oxide- and sulfide-based electrolytes, Wang *et al.* [22] discovered that body-centered-cubic anion sublattice enables a low migration barrier and fast ionic diffusion. He *et al.* [74] uncovered that a high concentration of mobile ions can activate the concerted migration, which has low activation energy. However, both features (the body-centered-cubic anion sublattice and the concerted migration) are absent in halide-based solid-state electrolytes. Therefore, the halide-based solid-state electrolytes achieve fast ionic diffusion through different mechanisms.

### 4.1 Facile ion migration in the close-packed anion sublattice of halide-based solid-state electrolytes

By probing $Li_3YCl_6$ (LYC, Figure 8a) and $Li_3YBr_6$ (LYB, Figure 8b) as example systems, Wang *et al.* [22] explored the diffusion mechanisms of halide-based solid-state electrolytes *via* first-principles calculations. *Ab initio* molecular dynamic simulations confirm that both materials have low activation energy (0.19 eV for LYC, Figure 8c; 0.28 eV for LYB, Figure 8d). LYB has a face-centered-cubic (FCC) anion sublattice, which enables its isotropic lithium diffusion. The hexagonal close-packed (HCP) anion sublattice of LYC leads to anisotropic ionic diffusion. Despite its fast diffusion along the *c*-axis, LYC is also prone to anti-site defect formation, which results in a blocking effect on lithium diffusion and an increase in the activation energy.

First-principles calculations confirmed that despite having a close-packed anion sublattice, halide-based solid-state electrolytes can still achieve low activation energy. Assuming a typical lattice volume, the calculated migration barrier in an empty HCP chloride and bromide lattice is 0.25 and 0.29 eV, respectively. Similarly, the calculated migration barrier in an empty FCC chloride or bromide lattice is 0.28 eV. These numbers are consistent with the activation energy obtained from molecular dynamic simulations. Besides, concerted migration was not observed in molecular dynamic simulations. These results confirmed that the low migration barrier of single lithium-ion hopping is the

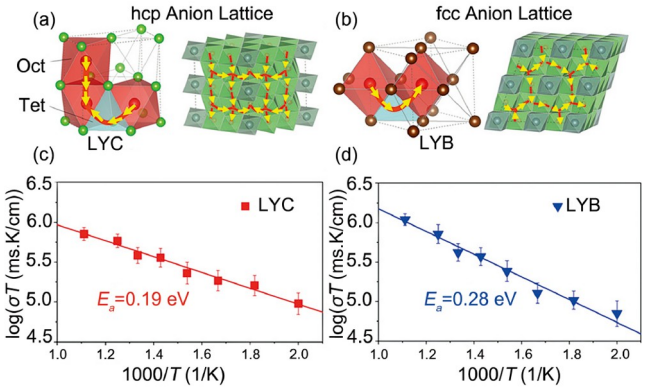


**Figure 8** (a) The Li-ion migration pathways in LYC. (b) The Li-ion migration pathways in LYB. (c) Arrhenius plot of $Li^+$ diffusivity in LYC from *ab initio* MD simulations. (d) Arrhenius plot of $Li^+$ diffusivity in LYB from *ab initio* MD simulations. (a–d) Reprinted with permission from Ref. [22], copyright 2019, Wiley-VCH (color online).

dominant factor of fast diffusion in halide-based solid-state electrolytes [22].

Since closed-pack anion sublattice is relatively common in crystal structures of ceramics, the unique low migration channels in halide-based materials imply a large design space for potential lithium superionic conductors. Based on these understandings, Wang *et al*. [22] proposed a series of halide-based materials as potential solid-state electrolyte materials through the computation, such as $Li_3ScCl_6$ and $Li_3HoCl_6$. These candidates have high room-temperature ionic conductivity, wide electrochemical windows, wide bandgap, and good compatibility with electrodes. Both materials and their doped variants were experimentally verified as potential solid-state electrolytes, which demonstrate the power of computation-driven discovery of novel battery materials [22]. Subsequently, Li *et al*. [23] assembled all-solid-state Li–Se batteries using $Li_3HoCl_6$ and $Li_3ScCl_6$ as solid-state electrolytes. Compared with conventional liquid electrolytes in Li–Se batteries, these halide-based solid-state electrolytes show the improved stability, less dissolution of Se, better interfacial compatibility, and suppressed decomposition of electrolytes and electrodes. Both computational and experimental analysis confirmed that chloride and bromide anions own high oxidation stability. The wide electrochemical stability windows and bandgap of chlorides- and bromides-based solid-state electrolytes makes it quite promising in all-solid-state batteries [21,22,46,69,72].

Yang *et al*. [75] systematically investigated $Li_3MX_6$ (M: multivalent cation; X: halogen anions) using high-throughput DFT calculations. They found that among the *oct-tet-oct* channels in the FCC anion sublattice and *oct-oct* channels in the HCP anion sublattice, the concentration and the distribution of Li-rich channels are important factors that govern Li kinetics in halide-based solid-state electrolytes. The Li-rich channels could suppress the negative influence from M cations in the lithium migration process in halide-based electrolytes. Their results also suggested promising candidates such as T1-$Li_3Ca_{0.5}Hf_{0.5}Cl_6$, T2-$Li_3ScBr_6$, T2-$Li_3ScCl_6$, T2-$Li_3YCl_6$, T2-$Li_3Y_{0.5}Sc_{0.5}Br_6$, T2-$Li_3Y_{0.5}Sc_{0.5}Br_6$, T3-$Li_3Mg_{0.5}Hf_{0.5}Cl_6$ and T4-$Li_3GaF_6$, which shows suitable characteristics as solid-state electrolytes.

### 4.2 Cation concentration and distribution modulates lithium diffusion in halide-based solid-state electrolytes

The distribution and configuration of cations is another important factor that significantly affects ionic conductivity in lithium-containing halide materials. In fact, the low migration barrier of lithium ions in a typical chloride or bromide anion sublattice is a necessary but not a sufficient condition for fast ionic diffusion. For example, $Li_2CdCl_4$ and $Li_2MgCl_4$ have a poor room-temperature ionic conductivity on the order of $10^{-6}$ S $cm^{-1}$ despite having a similar close-packed anion halide sublattice [76]. Therefore, understanding how the cation sublattice modulates lithium diffusion is crucial for the rational design and engineering of halide-based solid-state electrolyte materials.

By performing first-principles calculation on a large number of lithium-containing chlorides and their doped variants, Liu *et al*. [77] showed that the lithium diffusion is regulated by the cation concentration and cation distribution. In lithium-containing halide-based materials with a close-packed anion sublattice, the fraction of empty octahedral sites available for the lithium hopping is important to the lithium diffusion. They found that the optimal ratio between lithium sites and empty sites should be around 1. This optimal ratio explains why $Li_3MCl_6$ (M= In, Er, Sc) generally shows a good ionic conductivity as its stoichiometry is close to a ratio balance between lithium sites and vacant cation sites. By contrast, $Li_5MCl_8$ and $Li_6MCl_8$ (M is the non-Li metal cation) generally show poor ionic conductivity due to their insufficiency of available hopping sites.

In $Li_xMCl_y$-based (M is the non-Li metal cation) chlorides, the distribution of M cations modulates the energy barrier of lithium migration. The M cations, which are usually high-valance cations, alter the energy landscape of their nearby sites. Although the lithium diffusion can occur with a low migration barrier in an empty chloride sublattice, the distribution of M cations can increase the on-site energy of nearby octahedral sites, leading to a blocking effect on the lithium diffusion. Nudged elastic band (NEB) calculations confirmed that M cations can significantly increase the on-site energy of nearby vacant sites. This modulation effect from cations explains why $Li_2MCl_4$ (M=Cd, Mg) is also generally not a good ionic conductor, as the higher concentration of metal cations elevates the on-site energy of hopping sites, and thus increases the activation energy as well. The undesirable blocking effect from cations can be mitigated by low concentration or sparse configuration of the

metal cations [77]. Subsequently, Liang *et al*. [21,78] experimentally synthesized a series of $Li_xScCl_{3+x}$-based ($x$=2.5, 3, 3.5, and 4) solid-state electrolytes in close cubic-packed anion sublattices with the only difference in their composition (Li/Sc ratio). Through the experimental investigation, they found that $Li_xScCl_{3+x}$ has highly preferred structural orientation, high ionic conductivity over $10^{-3}$ S cm$^{-1}$ under room temperature and good electrochemical stability. They also performed DFT calculations to study the underlying mechanism (Figure 9a–d). *Ab initio* MD simulations show that when Li concentration is low, $Sc^{3+}$ ions exhibit the blocking effect by repelling lithium ions from entering its neighboring tetrahedral sites (Figure 9e) as the radial distribution function of Sc–Li pairs shows that no $Li^+$ density probability signal appears at its nearest neighboring tetrahedral sites at ~2.3 Å (Figure 9f). As $x$ increases, the carrier concentration increases, while the blocking effect from $Sc^{3+}$ decreases. These synergetic effects lead to high ionic conductivity and improved performance (Figure 9g).

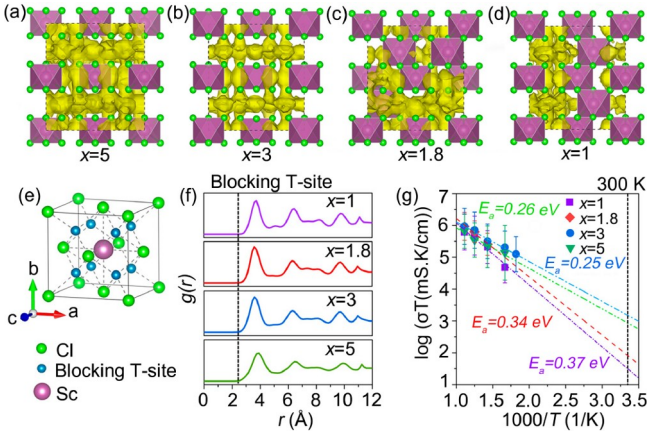


**Figure 9** The $Li^+$ probability density marked as yellow isosurfaces of different $Li_xScCl_{3+x}$ structures from AIMD simulations. (a) $Li_5ScCl_8$ ($x$ = 5). (b) $Li_3ScCl_6$ ($x$ = 3). (c) $Li_{1.8}ScCl_{4.8}$ ($x$ = 1.8). (d) $LiScCl_4$ ($x$ = 1) structures. (e) The blocking effect of Sc from the strong repellency between Sc and Li. (f) The radial distribution function of Sc–Li pairs shows that no $Li^+$ density probability signal appears at the nearest neighboring tetrahedral sites at ~2.3 Å. (g) Arrhenius plot of $Li^+$ diffusivity in $Li_xScCl_{3+x}$ ($x$ = 1, 1.8, 3, and 5) from simulations. (a–g) Reprinted with permission from Ref. [21], Copyright 2020, American Chemical Society (color online).

## 5 Liquid electrolytes

The electrolyte, which serves as both ionic conductors and electronic insulators, is an indispensable part of rechargeable batteries. Although solid-state electrolytes are attracting increasing attention, currently liquid electrolytes still dominate commercial batteries due to their high ionic conductivity and mature industrial process [2]. The pursuit of next-generation high-energy-density batteries appeals to high-voltage cathodes and alkali metal anodes, which puts forward very high requirements for electrolytes. In general, advanced electrolytes are highly supposed to meet the following requirements [79–81]:

(1) High electrochemical stability: a wide electrochemical window to resist the decomposition of electrolytes on electrodes.

(2) High thermal stability: high boiling point and nonflammable.

(3) High chemical stability: chemical inertness with other species or components in batteries.

(4) High ionic conductivity and diffusivity: ability to achieve high-rate performance.

(5) Compatibility with high-capacity electrodes: suppression of dendritic growth from alkali metal anodes.

(6) Low expense: a key requirement from commercialized applications.

(7) Environmental friendliness.

Tremendous efforts have been devoted to developing advanced liquid electrolytes, in which theoretical simulations are playing an increasingly important role and even constructing a new computation-driven electrolyte design paradigm [19,82,83]. Beyond conventional trial-and-error approaches, the computation-driven methods have been applied to the rational design of new electrolyte solvents, salts, and additives.

### 5.1 Solvents

The electrochemical stability of solvents is one of the most important parameters for electrolyte design, especially for lithium and sodium metal anodes. A stable solvent is beneficial to stabilize reactive anodes and deliver a long lifespan. The reduction potential is a fundamental descriptor to evaluate the reductive stability of solvents. Park *et al*. [84–86] adopted DFT calculations to determine the reduction potentials of electrolyte solvents and screened out 22 stable solvents against lithium metal anodes with a reduction potential smaller than −0.5 V *vs*. Li/$Li^+$ (Figure 10). The solvent reduction stability is highly related to their functional groups. For example, all the low-permittivity electron donor solvents present low reduction potentials, which mainly include linear ethers, cyclic ethers, and aromatic ethers. Only 4 of 14 aprotic protophilic solvents are predicted to be stable with lithium metal anodes. Beyond theoretical calculations, the authors further conducted experiments to evaluate the performance of theoretically screened solvents, including polyglyme, tetraglyme, and DME. A stable lithium metal anode in contact with the designed electrolyte delivered more than 100 cycles at a high areal capacity of 12 mAh cm$^{-1}$.

The solvent stability is highly dependent on the electrolyte solvation environment. Specifically, part of solvents is coordinated with cations in electrolytes, and their electrochemical stability changes due to the strong electron-

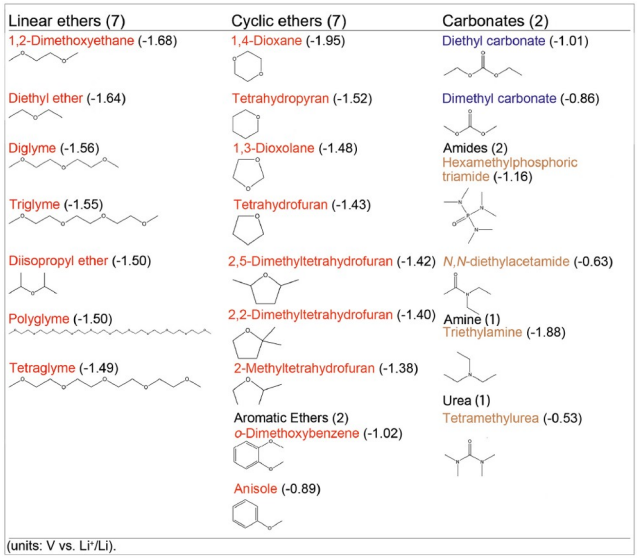


**Figure 10** Computation-screened molecules with a low reduction potential (<−0.5 V *vs*. Li/Li$^+$). The numbers in brackets denote the reduction potentials of corresponding solvents. The red, blue, and brown represent low-permittivity electron donors, aprotic protophobic, and aprotic protophilic solvents, respectively. Reprinted with permission from Ref. [84], copyright 2016, the Author(s) (color online).

withdrawing effects of cations. Zhang *et al*. [87] comprehensively probed the interaction between cations and solvents and developed the ion–solvent chemistry. Based on a systematic DFT calculation, the energy level of the lowest unoccupied molecular orbital (LUMO) of solvents in ion–solvent complexes is much lower than that of free solvents, indicating decreased reduction stability of solvents after interacting with cations. The LUMO energy change is positively related to the binding energy between solvents and cations, which is applied to various solvent and cation systems.

### 5.2 Salts

Salts are another important part of electrolytes, which dissolve in solvents and produce solvated ions as charge carriers. Ideal salts are supposed to have the following characteristics [80]:

(1) Good solubility in solvents and completely dissociated is preferred. The solvated ions, especially working ions, should have a high diffusivity and a high ionic conductivity.

(2) Good electrochemical stability of salt anions: inactive to be reduced or oxidized on the electrode surface or can form stable solid-state electrolyte interphase on the electrode surface.

(3) Good chemical stability of salt anions: inactive with other battery components, including electrolyte solvents, separators, electrodes, and packing materials.

(4) Good thermal stability: do not decompose under high temperatures.

(5) Low expense and environmental friendliness.

In fact, there are only limited available lithium salts that can work in lithium-ion batteries. Commonly used lithium salts include $LiPF_6$ (lithium hexafluorophosphate), LiTFSI (lithium *bis*(trifluoromethanesulfonyl)imide), LiFSI (lithium *bis*(fluorosulfonyl)imide), LiDFP (lithium difluorophosphate), LiBOB (lithium *bis*(oxalato)borate), and LiDFBOP (lithium difluorobis(oxalato) phosphate).

Among the above lithium salts, LiTFSI has been widely used for lithium metal batteries for its good solubility and excellent chemical and electrochemical stability. However, LiTFSI is hard to be modified to optimize its properties due to its chemical inertness. Johnson *et al*. [24] designed a series of fluorinated aryl sulfonamide tags (FAST) starting from TFSI-anions. The electrochemical stability, chemical stability, and dissociation property of FAST were investigated by both DFT calculations and experiments (Figure 11). As a result, the structure–function relationship of anions was obtained. The electrochemical and chemical stability of FAST is strongly related to the number of fluorine atoms in aromatic rings. Besides, other salt properties such as solubility, Lewis basicity, and ionic conductivity can be delicately regulated by changing the numbers and types of nucleophilic functional groups in FASTs.

By the computation, the higher computed electrochemical oxidation stability and higher average aromatic carbon charge, $c_+$ for FAST salts (**A**, **A-NeopF$_4$**, and **A-Neop$_2$F$_3$** (Figure 11)) evaluated by Natural Population Analysis (NPA) using DFT calculation could be correlated well with each other. From the experiment of several FAST salts in oxygenated atmosphere, the FAST salts (**A**, **A-ONeopF$_4$**, **A-ONop$_2$F$_3$** and **A-ONeop$_3$F$_2$**) show strong ability against the oxidation with only 2% fluorine atoms and 6% ONeop substituents oxidized upon charging to 4.2 $V_{Li}$ and 4.5 $V_{Li}$. By comparison, the four different FAST salts show electrochemical oxidation roughly an order higher than TFSI upon charging to 4.5 V [24].

### 5.3 Additives

Although the typical ratio of additives in electrolytes is relatively small, they play a critical role in regulating the bulk and interfacial properties of electrolytes. Compared with solvents and salts, the choice of additives is much more diverse, which affords tremendous chances for advanced electrolyte design.

According to the charge states of additives, they can be generally classified into neutral molecules, anion additives, and cations additives. The former two types have been widely probed in rechargeable batteries. For example, FEC molecules are predicted to possess a lower LUMO than EC and DEC solvents [88]. As a result, FEC additives preferentially decomposed on lithium metal anodes and pro-

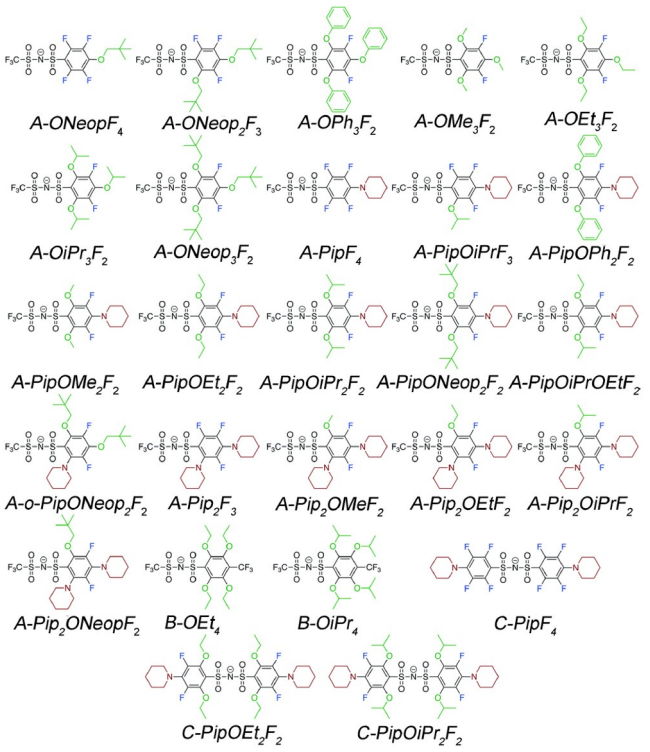


**Figure 11** The molecular structure of designed FAST anions. OPh: phenoxide; Pip: piperidine. Reprinted with permission from Ref. [24], copyright 2018, the Royal Society of Chemistry (color online).

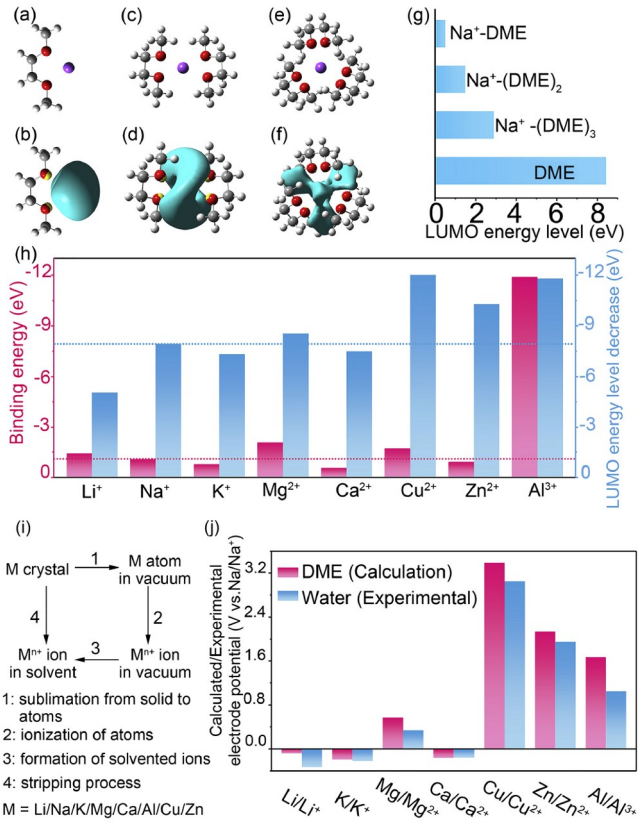


**Figure 12** Design principles for cation additives. (a–f) The geometrical structure and corresponding isosurface of LUMO of $Na^+$–$(DME)_n$ complexes. The hydrogen, carbon, oxygen, and sodium atoms are marked with white, gray, red, and purple, respectively. The cyan and yellow regions represent the positive and negative parts of the LUMO isosurface, respectively (isovalue: 0.03). (g) The comparison of LUMO energy levels of $Na^+$–$(DME)_n$ complexes and DME molecules. (h) The comparison of binding energy and LUMO energy decrease of ion–$(DME)_n$ complexes. (i) The thermodynamic cycle of calculating electrode potential. (j) The comparison of calculated or experimental electrode potentials of the considered metal/cation pairs. (a–j) Reprinted with permission from Ref. [93], copyright 2022, Elsevier (color online).

duced a LiF-rich SEI, which could impede interfacial side reactions and depress the dendritic growth of lithium metal anodes. Similar to FEC, $LiNO_3$ has also been widely adopted, especially for lithium–sulfur batteries, and can stabilize lithium metal anodes [89–91]. Because of the low solubility of $LiNO_3$ in conventional solvents, increasing the amount of $LiNO_3$ in electrolytes is a recent hot topic in lithium metal batteries.

There is plenty of room remaining for the exploration of cation additives and their distinctive functions have been verified. In 2013, Zhang *et al*. [92] reported $Cs^+$ as additives for lithium metal batteries, which can impede the dendritic growth through the electrostatic shield effect. Very recently, Chen *et al*. [93] established the principles to rationally select cation additives for metal anodes based on the ion–solvent chemistry (Figure 12). The screening rules are provided as follows:

(1) The cation additive should produce more stable ion–solvent complexes than working ions to improve electrolyte stability.

(2) The cation additive should possess a lower reduction potential than working ions, which not only prevents the consumption of additives but also impedes the dendritic growth of metal anodes through electrostatic shield effects.

(3) The cation additive should have larger binding energy with solvents than working ions. The third rule is not essential but beneficial to forming an electrostatic shield layer on anodes.

Cation–solvent complex model (Figure 12a–f) was adopted to probe the regulation of cations on solvent-reductive stability. All the three rules can be quantitatively described by easily accessed parameters in DFT calculations, that is the LUMO energy level (Figure 12g), binding energy (Figure 12h), and reduction potential (Figure 12j). After a systematic computation of potential cations, lithium ions satisfy all the rules for sodium metal batteries. The functions of $Li^+$ cation additives were further demonstrated by *in-situ* optical microscopic observations and electrochemical tests [19].

### 5.4 Ion transport mechanisms in the solvent system

The most important and fundamental function of liquid

electrolytes is ionic transport. In liquid electrolytes, both the cation and anion transport under electrochemical potentials, and their transport behaviors are largely determined by their interactions with solvents [19]. Classical MD simulations are powerful tools to build a relationship between the macroscopic properties and microscopic mechanisms [19,94].

In liquid electrolytes, the transport mechanisms can be classified into vehicular diffusion mechanism and structural diffusion mechanism [19]. In the vehicular mechanism, ions and species diffuse in a concerted fashion with their solvation shells (Figure 13a). By contrast, the structural diffusion mechanism (also known as ion-hopping mechanism) refers to the mode in which ions jump from one solvation shell to another solvation shell (Figure 13b). Both diffusion mechanisms are activated and contribute to the ion transport in liquid electrolytes. (Figure 13c). For example, Persson *et al.* [95] performed MD simulations of $LiPF_6$ and $LiBF_4$ in propylene carbonate at different concentrations. By analyzing diffusion modes and residence time, they quantified the contribution from each ion diffusion mode and elucidated how the salt concentration and different anion species can affect the diffusion modes.

By using polarizable force fields, Dmitry *et al.* [94] demonstrated that the ionic conductivity of ionic liquid-based electrolytes could be significantly improved by adding two organic solvents (acetonitrile (AN) or ethylene carbonate (EC)). MD simulations reveal that AN and EC can compete against $Ntf_2$ anions to coordinate with the $Li^+$ cations. The incorporation of AN and EC changes the binding pattern and the residence time of $Li^+$–$Ntf_2$ weakens $Li^+$–$N^{Ntf2}$ correlations, enhances the structural diffusion modes of $Li^+$ ions, and thus significantly enhances ion mobility and diffusion coefficient [94].

By combining MD simulations with electrochemical, neutron scattering and spectroscopic experimental techniques, Xu *et al.* [83] investigated the ion solvation and transport in the LiTFSI–$H_2O$ system at a wide range of concentrations. The results show that $Li^+$ ions will undergo solvation disproportionation at high salt concentrations (Figure 13d). The inhomogeneous $Li^+$ distribution will create TFSI-rich domains and $Li^+(H_2O)_4$ domain networks. The former will immobilize the anion while the latter domain could serve as a 3D percolating channel for fast $Li^+$ transport with a high transference number (Figure 13e).

Watanabe *et al.* [82] challenged the conventional $Li^+$ hopping models (*e.g.*, Onsagr's theory and Stokes' law) existing in high-concentration liquid electrolytes composed of $LiBF_4$ and sulfolane (SL). They tested the self-diffusion coefficients of $Li^+$ ($D_{Li}$), $BF_4^-$ ($D_{BF_4^-}$) and SL ($D_{SL}$) of concentrated electrolytes (SL/$LiBF_4$≤3, in molar ratio) using pulsed-field gradient NMR, while the results showed that $D_{SL}/D_{Li}$ and $D_{BF_4^-}/D_{Li}$ became lower than 1. The reversion in molar ratio and self-diffusion coefficients ratio suggested the

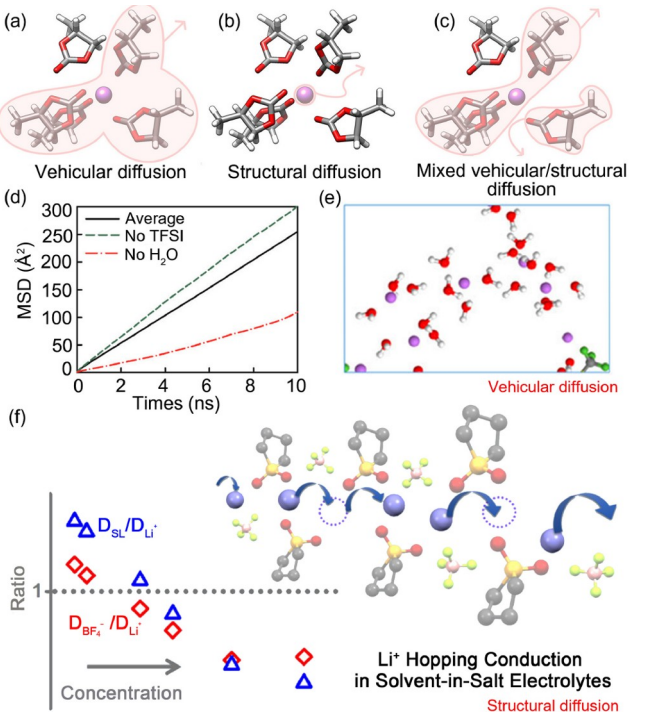


**Figure 13** (a) Vehicular diffusion. (b) Structural diffusion. (c) Mixture of vehicular and structural diffusion. O, C, H and Li atoms are shown as red, gray, white, and purple spheres, respectively. (d) The mean squared displacements (MSDs) of $Li^+$ cation for 21 m LITFSI–$H_2O$ for all $Li^+$ cation. (e) Representative $Li^+(H_2O)_n$ clusters from simulations at 21 m. (f) the $Li^+$ hopping conduction in solvation-in-salt electrolytes. (a–c) Reprinted with permission from Ref. [95], copyright 2019, American Chemistry Society. (d, e) Reprinted with permission from Ref. [83], copyright 2017, American Chemistry Society. (f) Reprinted with permission from Ref. [82], copyright 2018, American Chemistry Society (color online).

faster diffusion of $Li^+$ than SL and $BF_4^-$ in the liquids, thus the evolution of $Li^+$ hopping conduction. A higher $Li^+$ diffusion coefficient than SL and $BF_4^-$ in the highly concentrated $LiBF_4$–SL ($LiBF_4$/SL≥3) electrolytes is also reproduced through MD simulations, which is corroborated well with experiment results. Furthermore, they elucidated that $Li^+$ ion hopping from one coordinate to another with the ligand exchange in the highly concentrated electrolytes (Figure 13f). The $Li^+$ hopping conduction could effectively suppress the concentration polarization in a lithium battery.

## 6 Summary and outlook

In this review, we selected a few recent representative examples of computation-driven material developments in rechargeable lithium-ion batteries. These successful examples demonstrate that atomistic modeling and first-principles calculations can provide insightful understandings and practical design strategies, which eventually leads to the discovery of novel battery materials with improved performance. In fact, the continuous optimization of battery materials centers on a few important chemical properties, such

as ionic conductivity, chemical and electrochemical stability, reduction and oxidation potentials, and thermal stability. And these properties are largely determined by the atomistic structures of the materials. Therefore, by uncovering the underlying relationship between the structures and properties, atomistic modeling provides a computation-driven paradigm targeting the desirable chemical properties, which can significantly accelerate the discovery of novel electrode and electrolyte materials.

Despite the achievements, the computation-driven approaches to material discovery still confront many challenges. Successful material discoveries rely on accurate calculations and reliable predictions of material properties. However, the state-of-the-art computation scheme can be inaccurate or even incapable when calculating certain important properties. For example, *ab initio* MD simulations are widely used to acquire diffusion properties of electrolytes and electrodes, but they can only be performed under high temperatures and in small systems. The effect from complex structures (such as grain boundaries) or at room temperature (such as low-temperature phase transformation) would be challenging to be probed. Recently, machine learning played an increasingly important role in material discovery and design. In particular, machine learning force fields, which are trained on datasets generated by first-principles calculations, have the potential to significantly accelerate MD simulations without compromising on accuracy [96,97]. The machine learning force fields have been successfully demonstrated in a few solid-state electrolyte material systems [98,99]. They can potentially extend the temporal and spatial scale of AIMD simulations and enable us to study complex structures or low-temperature processes in battery materials [100]. Design principles for the optimization of high-voltage cathode materials, such as Ni-rich NMC materials, is in urgent need. However, the complexity of multiply coupled processes that involve the high-voltage cycling, including surface reconstruction, anion redox, and cation mixing, hinders the discovery of rational design rules. Anodes are also the indispensable part for lithium-ion batteries. Despite a few recent computation-driven material designs [101–104], the complicated coupling of chemical, electrochemical, and mechanical processes at the anode–electrolyte interface still pose a lot of challenges. Developing accurate and highly efficient models for predicting physiochemical properties of various molecular and liquid electrolytes such as redox potential and viscosity in solvation environments and working electrochemical conditions is still challenging. While the softness of materials quantified by the phonon band center was demonstrated as an efficient descriptor to discover fast ionic conductors, the explicit correlation between ionic diffusion and certain vibration modes is still unclear, which impedes the exploration of promising conductors by identifying or stimulating the certain phonon mode. Thermodynamic analysis is commonly used to assess the synthesizability of predicted solid-state electrolytes or electrode materials. Nevertheless, it is usually insufficient to formulate synthesis recipes merely based on thermodynamic analysis, as the kinetics plays an important role in the synthesis process. Computation-guided synthesis is also an emerging field that attracts increasing research interest. We expect that as the computational approaches advance, computation-driven paradigm will bring more fundamental understandings and breakthrough discoveries of battery materials in the future.

**Acknowledgements** X.L. and Y.Z. would like to acknowledge funding support from the Research Center for industries of the Future (RCIF) at Westlake University and the start-up fund from Westlake University. X.C. appreciates the support from the National Natural Science Foundation of China (22109086), Young Elite Scientists Sponsorship Program by CAST (2021QNRC001), and the Shuimu Tsinghua Scholar Program of Tsinghua University. Q.B. acknowledged the support from the National Natural Science Foundation of China (22109113) and the Natural Science Foundation of Shanxi Province (20210302124105).

**Conflict of interest** The authors declare no conflict of interest.

1 Fang S, Bresser D, Passerini S. *Transition Metal Oxides for Electrochemical Energy Storage*. In: Nanda J, Augustyn V. *Transition Metal Oxide Anodes for Electrochemical Energy Storage in Lithium- and Sodium-ion Batteries*. Weiheim: Wiley-VCH, 2022. 55–90
2 Li M, Lu J, Chen Z, Amine K. *Adv Mater*, 2018, 30: 1800561
3 Whittingham MS. *Chem Rev*, 2014, 114: 11414–11443
4 Mizushima K, Jones PC, Wiseman PJ, Goodenough JB. *Mater Res Bull*, 1980, 15: 783–789
5 Thackeray MM, Johnson PJ, de Picciotto LA, Bruce PG, Goodenough JB. *Mater Res Bull*, 1984, 19: 179–187
6 Padhi AK, Nanjundaswamy KS, Masquelier C, Goodenough JB. *J Electrochem Soc*, 1997, 144: 2581–2586
7 Fong R, von Sacken U, Dahn JR. *J Electrochem Soc*, 1990, 137: 2009–2013
8 Kamaya N, Homma K, Yamakawa Y, Hirayama M, Kanno R, Yonemura M, Kamiyama T, Kato Y, Hama S, Kawamoto K, Mitsui A. *Nat Mater*, 2011, 10: 682–686
9 Murugan R, Thangadurai V, Weppner W. *Angew Chem Int Ed*, 2007, 46: 7778–7781
10 Fan X, Wang C. *Chem Soc Rev*, 2021, 50: 10486–10566
11 Zhang X, Tang B, Zhou Z. *Green Energy Environ*, 2021, 6: 3–4
12 Jain A, Shin Y, Persson KA. *Nat Rev Mater*, 2016, 1: 15004
13 Sun Y, Yang T, Ji H, Zhou J, Wang Z, Qian T, Yan C. *Adv Energy Mater*, 2020, 10: 2002373
14 Urban A, Seo DH, Ceder G. *npj Comput Mater*, 2016, 2: 16002
15 Nolan AM, Zhu Y, He X, Bai Q, Mo Y. *Joule*, 2018, 2: 2016–2046
16 Meng YS, Arroyo-de Dompablo ME. *Energy Environ Sci*, 2009, 2: 589–609
17 Kirklin S, Meredig B, Wolverton C. *Adv Energy Mater*, 2013, 3: 252–262
18 Ceder G. *MRS Bull*, 2010, 35: 693–701
19 Yao N, Chen X, Fu ZH, Zhang Q. *Chem Rev*, 2022, 122: 10970–11021
20 Shevlin S, Castro B, Li X. *Nat Mater*, 2021, 20: 727
21 Liang J, Li X, Wang S, Adair KR, Li W, Zhao Y, Wang C, Hu Y, Zhang L, Zhao S, Lu S, Huang H, Li R, Mo Y, Sun X. *J Am Chem Soc*, 2020, 142: 7012–7022
22 Wang S, Bai Q, Nolan AM, Liu Y, Gong S, Sun Q, Mo Y. *Angew Chem Int Ed*, 2019, 58: 8039–8043

23 Li X, Liang J, Kim JT, Fu J, Duan H, Chen N, Li R, Zhao S, Wang J, Huang H, Sun X. *Adv Mater*, 2022, 34: 2200856
24 Huang M, Feng S, Zhang W, Giordano L, Chen M, Amanchukwu CV, Anandakathir R, Shao-Horn Y, Johnson JA. *Energy Environ Sci*, 2018, 11: 1326–1334
25 Lun Z, Ouyang B, Kwon DH, Ha Y, Foley EE, Huang TY, Cai Z, Kim H, Balasubramanian M, Sun Y, Huang J, Tian Y, Kim H, McCloskey BD, Yang W, Clément RJ, Ji H, Ceder G. *Nat Mater*, 2021, 20: 214–221
26 Zhou L, Zuo TT, Kwok CY, Kim SY, Assoud A, Zhang Q, Janek J, Nazar LF. *Nat Energy*, 2022, 7: 83–93
27 Li X, Liang J, Chen N, Luo J, Adair KR, Wang C, Banis MN, Sham TK, Zhang L, Zhao S, Lu S, Huang H, Li R, Sun X. *Angew Chem Int Ed*, 2019, 58: 16427–16432
28 Clément RJ, Lun Z, Ceder G. *Energy Environ Sci*, 2020, 13: 345–373
29 Liu W, Oh P, Liu X, Lee MJ, Cho W, Chae S, Kim Y, Cho J. *Angew Chem Int Ed*, 2015, 54: 4440–4457
30 Kim UH, Jun DW, Park KJ, Zhang Q, Kaghazchi P, Aurbach D, Major DT, Goobes G, Dixit M, Leifer N, Wang CM, Yan P, Ahn D, Kim KH, Yoon CS, Sun YK. *Energy Environ Sci*, 2018, 11: 1271–1279
31 Shi Y, Xing Y, Kim K, Yu T, Lipson AL, Dameron A, Connell JG. *J Electrochem Soc*, 2021, 168: 040501
32 Wandt J, Freiberg ATS, Ogrodnik A, Gasteiger HA. *Mater Today*, 2018, 21: 825–833
33 Xu GL, Liu Q, Lau KKS, Liu Y, Liu X, Gao H, Zhou X, Zhuang M, Ren Y, Li J, Shao M, Ouyang M, Pan F, Chen Z, Amine K, Chen G. *Nat Energy*, 2019, 4: 484–494
34 Stoyanova R. *Solid State Ion*, 2003, 161: 197–204
35 Urban A, Lee J, Ceder G. *Adv Energy Mater*, 2014, 4: 1400478
36 Lee J, Urban A, Li X, Su D, Hautier G, Ceder G. *Science*, 2014, 343: 519–522
37 Van der Ven A, Bhattacharya J, Belak AA. *Acc Chem Res*, 2013, 46: 1216–1225
38 Ji H, Urban A, Kitchaev DA, Kwon DH, Artrith N, Ophus C, Huang W, Cai Z, Shi T, Kim JC, Kim H, Ceder G. *Nat Commun*, 2019, 10: 592
39 Urban A, Abdellahi A, Dacek S, Artrith N, Ceder G. *Phys Rev Lett*, 2017, 119: 176402
40 Lee J, Seo DH, Balasubramanian M, Twu N, Li X, Ceder G. *Energy Environ Sci*, 2015, 8: 3255–3265
41 Zhao Q, Stalin S, Zhao CZ, Archer LA. *Nat Rev Mater*, 2020, 5: 229–252
42 Sun YK. *ACS Energy Lett*, 2020, 5: 3221–3223
43 Zhu Y, He X, Mo Y. *ACS Appl Mater Interfaces*, 2015, 7: 23685–23693
44 Tanibata N, Takimoto S, Nakano K, Takeda H, Nakayama M, Sumi H. *ACS Mater Lett*, 2020, 2: 880–886
45 Gordiz K, Muy S, Zeier WG, Shao-Horn Y, Henry A. *Cell Rep Phys Sci*, 2021, 2: 100431
46 Kwak H, Wang S, Park J, Liu Y, Kim KT, Choi Y, Mo Y, Jung YS. *ACS Energy Lett*, 2022, 7: 1776–1805
47 Wang K, Ren Q, Gu Z, Duan C, Wang J, Zhu F, Fu Y, Hao J, Zhu J, He L, Wang CW, Lu Y, Ma J, Ma C. *Nat Commun*, 2021, 12: 4410
48 Wang Y, Richards WD, Ong SP, Miara LJ, Kim JC, Mo Y, Ceder G. *Nat Mater*, 2015, 14: 1026–1031
49 Lin YY, Yong AXB, Gustafson WJ, Reedy CN, Ertekin E, Krogstad JA, Perry NH. *Curr Opin Solid State Mater Sci*, 2020, 24: 100875
50 Ohno S, Banik A, Dewald GF, Kraft MA, Krauskopf T, Minafra N, Till P, Weiss M, Zeier WG. *Prog Energy*, 2020, 2: 022001
51 Wang C, Xu BB, Zhang X, Sun W, Chen J, Pan H, Yan M, Jiang Y. *Small*, 2022, 18: 2107064
52 Kraft MA, Culver SP, Calderon M, Böcher F, Krauskopf T, Senyshyn A, Dietrich C, Zevalkink A, Janek J, Zeier WG. *J Am Chem Soc*, 2017, 139: 10909–10918
53 Culver SP, Koerver R, Krauskopf T, Zeier WG. *Chem Mater*, 2018, 30: 4179–4192
54 Muy S, Bachman JC, Giordano L, Chang HH, Abernathy DL, Bansal D, Delaire O, Hori S, Kanno R, Maglia F, Lupart S, Lamp P, Shao-Horn Y. *Energy Environ Sci*, 2018, 11: 850–859
55 Muy S, Voss J, Schlem R, Koerver R, Sedlmaier SJ, Maglia F, Lamp P, Zeier WG, Shao-Horn Y. *iScience*, 2019, 16: 270–282
56 Schlem R, Muy S, Prinz N, Banik A, Shao-Horn Y, Zobel M, Zeier WG. *Adv Energy Mater*, 2020, 10: 1903719
57 Kanno R, Murayama M. *J Electrochem Soc*, 2001, 148: A742
58 Muy S, Bachman JC, Chang HH, Giordano L, Maglia F, Lupart S, Lamp P, Zeier WG, Shao-Horn Y. *Chem Mater*, 2018, 30: 5573–5582
59 Di Stefano D, Miglio A, Robeyns K, Filinchuk Y, Lechartier M, Senyshyn A, Ishida H, Spannenberger S, Prutsch D, Lunghammer S, Rettenwander D, Wilkening M, Roling B, Kato Y, Hautier G. *Chem*, 2019, 5: 2450–2460
60 Martínez-Juárez A, Pecharromán C, Iglesias JE, Rojo JM. *J Phys Chem B*, 1998, 102: 372–375
61 Schlem R, Ghidiu M, Culver SP, Hansen AL, Zeier WG. *ACS Appl Energy Mater*, 2019, 3: 9–18
62 Kong ST, Deiseroth HJ, Maier J, Nickel V, Weichert K, Reiner C. *Z anorg allg Chem*, 2010, 636: 1920–1924
63 Schlem R, Bernges T, Li C, Kraft MA, Minafra N, Zeier WG. *ACS Appl Energy Mater*, 2020, 3: 3684–3691
64 Sagotra AK, Chu D, Cazorla C. *Phys Rev Mater*, 2019, 3: 035405
65 Yelon A, Movaghar B, Branz HM. *Phys Rev B*, 1992, 46: 12244–12250
66 Metselaar R, Oversluizen G. *J Solid State Chem*, 1984, 55: 320–326
67 Chen R, Xu Z, Lin Y, Lv B, Bo SH, Zhu H. *ACS Appl Energy Mater*, 2021, 4: 2107–2114
68 Bartók AP, Kermode J, Bernstein N, Csányi G. *Phys Rev X*, 2018, 8: 041048
69 Asano T, Sakai A, Ouchi S, Sakaida M, Miyazaki A, Hasegawa S. *Adv Mater*, 2018, 30: 1803075
70 Li X, Liang J, Luo J, Norouzi Banis M, Wang C, Li W, Deng S, Yu C, Zhao F, Hu Y, Sham TK, Zhang L, Zhao S, Lu S, Huang H, Li R, Adair KR, Sun X. *Energy Environ Sci*, 2019, 12: 2665–2671
71 Kwak H, Han D, Lyoo J, Park J, Jung SH, Han Y, Kwon G, Kim H, Hong ST, Nam KW, Jung YS. *Adv Energy Mater*, 2021, 11: 2003190
72 Liu Z, Ma S, Liu J, Xiong S, Ma Y, Chen H. *ACS Energy Lett*, 2020, 6: 298–304
73 Li X, Liang J, Yang X, Adair KR, Wang C, Zhao F, Sun X. *Energy Environ Sci*, 2020, 13: 1429–1461
74 He X, Zhu Y, Mo Y. *Nat Commun*, 2017, 8: 15893
75 Yang G, Liang X, Zheng S, Chen H, Zhang W, Li S, Pan F. *eScience*, 2022, 2: 79–86
76 Kanno R, Takeda Y, Yamamoto O. *Mater Res Bull*, 1981, 16: 999–1005
77 Liu Y, Wang S, Nolan AM, Ling C, Mo Y. *Adv Energy Mater*, 2020, 10: 2002356
78 Liang J, Li X, Adair KR, Sun X. *Acc Chem Res*, 2021, 54: 1023–1033
79 Yamada Y, Wang J, Ko S, Watanabe E, Yamada A. *Nat Energy*, 2019, 4: 269–280
80 Xu K. *Chem Rev*, 2004, 104: 4303–4418
81 Xu K. *Chem Rev*, 2014, 114: 11503–11618
82 Dokko K, Watanabe D, Ugata Y, Thomas ML, Tsuzuki S, Shinoda W, Hashimoto K, Ueno K, Umebayashi Y, Watanabe M. *J Phys Chem B*, 2018, 122: 10736–10745
83 Borodin O, Suo L, Gobet M, Ren X, Wang F, Faraone A, Peng J, Olguin M, Schroeder M, Ding MS, Gobrogge E, von Wald Cresce A, Munoz S, Dura JA, Greenbaum S, Wang C, Xu K. *ACS Nano*, 2017, 11: 10462–10471
84 Park MS, Ma SB, Lee DJ, Im D, Doo SG, Yamamoto O. *Sci Rep*, 2015, 4: 3815
85 Chen X, Shen X, Li B, Peng H-, Cheng X-, Li B-, Zhang X-, Huang J-, Zhang Q. *Angew Chem Int Ed*, 2018, 57: 734–737
86 Chen X, Yao N, Zeng BS, Zhang Q. *Fundamental Res*, 2021, 1: 393–

398
87 Chen X, Li HR, Shen X, Zhang Q. *Angew Chem Int Ed*, 2018, 57: 16643–16647
88 Zhang XQ, Cheng XB, Chen X, Yan C, Zhang Q. *Adv Funct Mater*, 2017, 27: 1605989
89 Shi Q, Zhong Y, Wu M, Wang H, Wang H. *Proc Natl Acad Sci USA*, 2018, 115: 5676–5680
90 Fu J, Ji X, Chen J, Chen L, Fan X, Mu D, Wang C. *Angew Chem Int Ed*, 2020, 59: 22194–22201
91 Li W, Yao H, Yan K, Zheng G, Liang Z, Chiang YM, Cui Y. *Nat Commun*, 2015, 6: 7436
92 Ding F, Xu W, Graff GL, Zhang J, Sushko ML, Chen X, Shao Y, Engelhard MH, Nie Z, Xiao J, Liu X, Sushko PV, Liu J, Zhang JG. *J Am Chem Soc*, 2013, 135: 4450–4456
93 Chen X, Shen X, Hou TZ, Zhang R, Peng HJ, Zhang Q. *Chem*, 2020, 6: 2242–2256
94 Li Z, Borodin O, Smith GD, Bedrov D. *J Phys Chem B*, 2015, 119: 3085–3096
95 Self J, Fong KD, Persson KA. *ACS Energy Lett*, 2019, 4: 2843–2849
96 Deringer VL, Caro MA, Csányi G. *Adv Mater*, 2019, 31: 1902765
97 Unke OT, Chmiela S, Sauceda HE, Gastegger M, Poltavsky I, Schütt KT, Tkatchenko A, Müller KR. *Chem Rev*, 2021, 121: 10142–10186
98 Pollice R, dos Passos Gomes G, Aldeghi M, Hickman RJ, Krenn M, Lavigne C, Lindner-D'Addario M, Nigam AK, Ser CT, Yao Z, Aspuru-Guzik A. *Acc Chem Res*, 2021, 54: 849–860
99 Huang JX, Csányi G, Zhao JB, Cheng J, Deringer VL. *J Mater Chem A*, 2019, 7: 19070–19080
100 Zhu Z, Zhu Y. *Acc Mater Res*, 2022, 3: 1101–1105
101 Wang A, Kadam S, Li H, Shi S, Qi Y. *npj Comput Mater*, 2018, 4: 15
102 Zhang H, Yang Y, Ren D, Wang L, He X. *Energy Storage Mater*, 2021, 36: 147–170
103 Yang M, Liu Y, Nolan AM, Mo Y. *Adv Mater*, 2021, 33: 2008081
104 Zhang X, Yang Y, Zhou Z. *Chem Soc Rev*, 2020, 49: 3040–3071